2-20-2008

Electronic and magnetic properties of endohedrally doped fullerene $Mn@C_{60}$: A total energy study

Guangping Li
University of Nebraska at Omaha, Omaha, Nebraska

R. F. Sabirianov
University of Nebraska at Omaha, Omaha, Nebraska

Jing Lu
University of Nebraska at Omaha, Omaha, Nebraska

Xiao Cheng Zeng
University of Nebraska-Lincoln, xzeng1@unl.edu

W. N. Mei
University of Nebraska at Omaha, Omaha, Nebraska

Electronic and magnetic properties of endohedrally doped fullerene $Mn@C_{60}$: A total energy study

Guangping Li[a] and R. F. Sabirianov
Department of Physics, University of Nebraska at Omaha, Omaha, Nebraska 68182-0266, USA

Jing Lu
Department of Physics, University of Nebraska at Omaha, Omaha, Nebraska 68182-0266, USA and Mesoscopic Physics Laboratory, Department of Physics, Peking University, Beijing 100871, People's Republic of China

X. C. Zeng
Department of Chemistry, University of Nebraska-Lincoln, Lincoln, Nebraska 68588-0304, USA

W. N. Mei
Department of Physics, University of Nebraska at Omaha, Omaha, Nebraska 68182-0266, USA

(Received 20 September 2007; accepted 2 December 2007; published online 20 February 2008)

We perform total energy calculations on a manganese atom encapsulated inside a C_{60} cage using density functional theory with the generalized gradient approximation through three optimization schemes and along four paths inside the cage. We find that when Mn is located in the central region, its electronic and magnetic properties are not exactly the same as those of a free Mn atom due to weak coupling between Mn and the cage. As Mn is shifted toward to the edge, the total energy and spin start to change significantly when Mn is situated about one-third of the way between the cage center and edge, and the total energy reaches a local minimum. Finally the interaction between Mn and the cage turns repulsive as Mn approaches the edge. We also find that, along the lowest energy path, there exist three consecutive local energy minima and each of these has a different spin M. The ground state has the lowest $M=3$, Mn is located about 1.6 Å away from the cage center, and the binding energy is 0.08 eV. We attribute the decrease in total energy and spin to Mn and C hybridization. © *2008 American Institute of Physics*. [DOI: 10.1063/1.2828535]

I. INTRODUCTION

Encapsulating atoms or molecules[1–3] inside a C_{60} has attracted attention for its scientific interest and practical applications. In the past several years, some work has been done on doping C_{60} and C_{82} using alkali, transition, and rare-earth metals[4–12] because of their valence level structures, such as ns, $(n-1)d$, and $(n-2)f$, which may exhibit different spin configurations. During endohedral doping, the fullerene functions as a protective screen and the properties of the dopant remain intact, for example, $Gd@C_{60}$ and $Gd_3N@C_{80}$ (Refs. 4 and 5) are recently considered as a new generation of magnetic resonance imaging contrast agents due to the high spin ground state of Gd while its toxicity is shielded by the fullerene.

In this work, we opt to study the electronic and magnetic properties of $Mn@C_{60}$ because Mn is a $3d$ transition metal with five d electrons in the outer shell d^5, hence it might serve as a good candidate for designing magnetic devices if the high spin configuration can be preserved as the ground state or if its different spins can be manipulated. In fact the system was studied before. Chang *et al.*[6] performed restricted Hartree-Fock calculations on $Mn@C_{60}$ with I_h symmetry, where Mn is located at the center of C_{60} cage, but their calculated binding energies are negative, meaning nonbinding between Mn and C_{60}, and rendering $Mn@C_{60}$ nonexistent. Lu *et al.*[7] carried out calculations on electron affinity and ionization potential for $Mn@C_{60}$ with I_h symmetry using the discrete variational local density functional method. They obtained the charge transfer from Mn to carbon cage as 0.72, i.e., $Mn^{0.72+}@C_{60}^{0.72-}$. However, to the best of our knowledge, there is no study on $Mn@C_{60}$ with Mn at off-center positions published whereas the experimental work of Heath *et al.* on LaC_{60} (Ref. 1) and the theoretical work of Laasonen *et al.* on $La@C_{82}$ (Ref. 8) and Andreoni and Curioni on $M@C_{60}$ (M=Na,K,Al,La,Y) (Ref. 9) have shown that the stable structures of $M@C_{60}$ and $M@C_{82}$ can have M off center. Heath *et al.* found that LaC_{60} is highly stable and the carbon cages have only one highly stable binding site in the carbon cage ligand.[1] In the work of Laasonen *et al.*, La is found to be located at a low-symmetry and highly coordinated site where the ground state of $La@C_{82}$ has three electrons transferred from La to C_{82}, i.e., $La^{3+}@C_{82}^{3-}$. In the work of Andreoni and Curioni,[10] La and Li are found to be located close to the center of a C_6 ring, and the binding energies are ~61 kcal/mol for $La@C_{60}$ and ~44 kcal/mol for $Li@C_{60}$, respectively. In the above-mentioned work, the total energy inside the carbon cages is not extensively studied.

Therefore, it is our purpose to investigate the binding energy and spin configuration of an encapsulated metal atom

[a]Author to whom correspondence should be addressed. FAX: (402) 554-3100. Electronic mail: gli@mail.unomaha.edu.

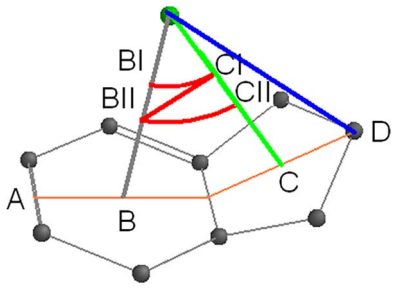

FIG. 1. (Color online) The four paths used in our calculations are defined as follows: paths 1, 2, and 3 are radial paths, starting from the cage center to a carbon atom (D), the center of a C_5 ring (C), and C_6 ring (B), respectively. Path 4 has two arcs of radii 1.2 (from the cage center to B_I or C_I) and 1.6 Å (from the cage center to B_{II} or C_{II}) and one straight line connecting B_{II} and C_I. The angular span between paths 2 and 3 is about 40°.

inside the fullerene using $Mn@C_{60}$ as a prototype. To accomplish the task we utilize three different computational programs and design three optimization schemes to describe the total energy variations through four different paths. In Sec. II, we illustrate the technical details regarding the computational methods and optimization schemes. In Sec. III, we show the results and our analysis. Finally in Sec. IV, we present our concluding remarks.

II. COMPUTATIONAL METHODS

In order to facilitate total energy calculations on a Mn inside a C_{60} cage, we devise four paths as shown in Fig. 1 The first three are radial paths that all start from the center of cage and end at the edge, namely, on one of the carbons (D), center of the C_5 ring (C), and C_6 ring (B), respectively. It is natural to speculate that there is at least one energy minimum on each path, and we also note that the energy minima on paths 2 and 3 are lower in energy than that on path 1. Hence in order to observe the angular variation of total energy, we design a fourth path that has two arcs of radii about 1.2 and 1.6 Å (the locations of local energy minima for paths 2 and 3, respectively) from the cage center and/or a straight line connecting these two local energy minima. Hence, according to the I_h symmetry of cage, moving Mn along these four paths will provide a complete description of Mn's total energy surface inside C_{60}.

Subsequently we portray how Mn is moved from one end of the path to the other, bearing in mind that the electronic configuration and total energy of the entire system $Mn@C_{60}$, not to mention its spin, vary simultaneously. We design three different optimization schemes to accommodate these different situations: First, only C_{60} is fully optimized using the molecular computational package GAUSSIAN 03 (G03)[13] at the B3LYP/6-31G* level (Beck's three parameter exchange functional[14] and Lee-Yang-Parr correlation functional[15]), which is a well-established method for geometric optimization and vibrational frequency calculation of compounds composed of only first and second row atoms. Then shifting the position of Mn inside an optimized cage, we calculate the total energy of $Mn@C_{60}$ using VASP (Vienna *ab initio* simulation package[16–20]) which has the advantage of allowing spin to relax. Second, C_{60} and Mn are optimized together using VASP and the molecular modeling program

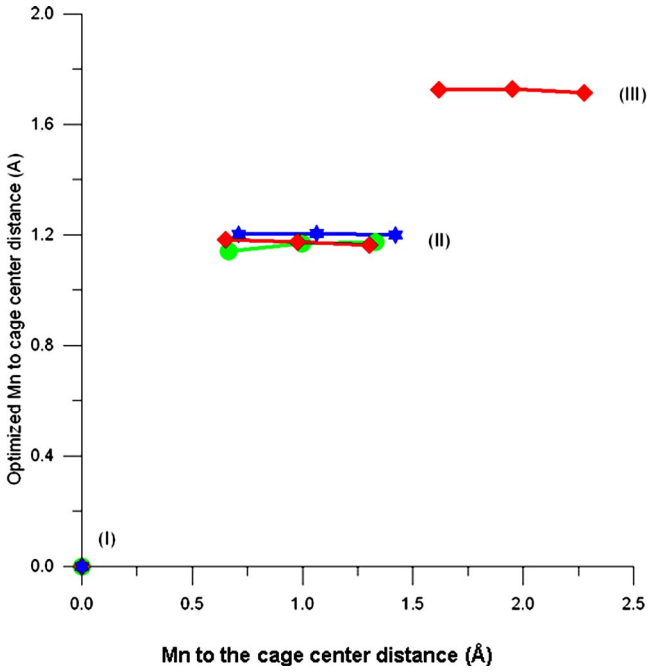

FIG. 2. (Color online) Input and optimized Mn to the cage center distances obtained using scheme 2 (full optimization). The total energy is set as zero when Mn is located at the cage center. The three local energy minima are (i) $M=5.7$, since Mn is located at the cage center before and after optimization, the energy is equal to zero. (ii) $M=5$: ⋆, along path 1, $E=-0.28$ eV; ●, along path 2, $E=-0.24$ eV; and ◆, along path 3, $E=-0.25$ eV. (iii) $M=3$, ◆ only, along path 3, $E=-0.45$ eV.

DMOL3 (density functional calculation on molecules_3 dimension of Materials Studio from Accelrys[21,22]) without symmetry restriction and we then compare these results with those of scheme 1. However, we find that, although scheme 2 is capable of depicting C_{60} structural change due to position variations of Mn, the outcomes of optimizations are always the nearby local energy minima in spite of the different starting positions shown in Fig. 2. Thus we design a third scheme, namely, $Mn@C_{60}$ is first fully optimized with Mn located at the center of the cage (I_h symmetry) to prevent possible structural rupture (C_{60} breakdown). Then when Mn is moved away from the center, the system undergoes partial optimization: one-half of C_{60} is allowed to relax, while the other half of C_{60} together with Mn is fixed using VASP, and the distances of Mn to the fixed half of the cage are kept constant. Henceforth we can determine how the half cage adjusts due to the movement of Mn and keep track of the energy change continuously. We expect that these three schemes together will provide a consistent description of the optimized $Mn@C_{60}$ geometries, local energy minima, and associated spins.

We utilize three computational packages to accomplish the fore-mentioned tasks. First, G03 at the B3LYP/6-31G* level is used to optimize C_{60}. G03 has geometric optimization and frequency calculation capability but allows only fixed spin (charge and spin multiplicity as input). Thus it is not suitable for studying Mn movement inside C_{60}, because the spin of $Mn@C_{60}$ changes along with the position of Mn. Second, VASP, incorporated with the generalized gradient approximation of density functional theory and the Perdew-

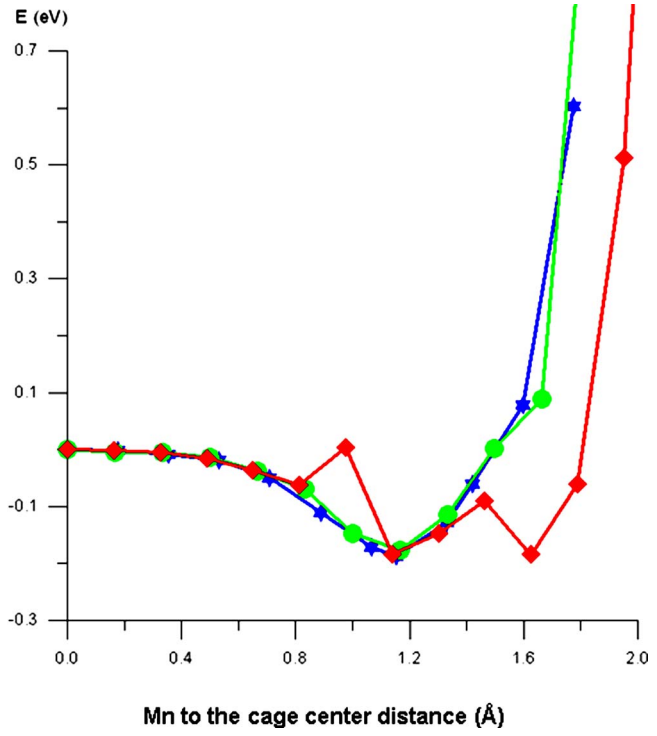

FIG. 3. (Color online) Total energy (eV) changes with Mn to the cage center distance (Å) along the radial paths 1 (⋆), 2 (●), and 3 (♦). The total energy is set as zero when Mn is located at the cage center. Note that there are three energy minima on path 3, but only one energy minimum on paths 2 and 1.

Burke-Ernzerhof (PBE) exchange and correlation functionals[23,24] plus projector augmented plane wave (PAW) method,[25,26] is used to optimize geometries and calculate total energies. VASP calculations allow the spin to relax when changing Mn position and during self-consistent field (SCF) iteration cycles, but it has no frequency calculation capability. Third is an all-electron calculation using DMOL3 with PBE and double numerical plus polarization (DNP) basis set,[27] by which we can efficiently calculate the total energy and optimize the geometry, in addition to relax spin during SCF iterations. Since VASP is designed to handle materials with periodic symmetries, we construct a super cell of $(15\times15\times15\ \text{Å}^3)$ with the C_{60} cage located at the center to simulate an isolated fullerene. In the VASP calculations, we use 941 192$(=98^3)$ plane waves but only one k point (the Γ point). The computational parameters such as energy cutoff for pseudopotentials, Gaussian broadening parameter, and the energy convergence criteria are set at 400 eV, 0.08 eV, and accurate, respectively.

III. RESULTS AND DISCUSSION

We first follow optimization scheme 1, that is, first optimize the structure of C_{60} using G03 at the B3LYP/6-31G* level, then vary the position of Mn along the three radial paths described in the previous section, and calculate single point total energies using VASP at the PBE/PAW level. During each step, we fix Mn at designated positions, about ten for each path, inside the optimized cage. As shown in Fig. 3, i.e., along path 3, when Mn is located in the central region, we notice that the energy variation is monotonic. This is a manifestation of weak coupling between Mn and cage. However, we find that the spin is 5.7, which is greater than that of a free Mn atom ($M=5$). Upon closer examination, we reveal that the electronic configuration of Mn is $[\text{Ar}]3d^{5.44}4s^{1.07}4p^{0.07}$ based on DMOL3 orbital and charge Mulliken population analysis. This means there is charge transfer from Mn's $4s$ level to its $3d$ and $4p$ orbitals, and about 0.42 Mn electrons are moved to the carbon cage. Based on a VASP calculation, we obtain the electronic configuration of Mn as $[\text{Ar}]3d^{5.13}4s^{0.52}4p^{0.03}$, which means that 1.32 Mn electrons are shifted to the cage. This electrostatic attraction tends to drag Mn toward to the edge. As Mn is moved toward to the edge, the total energy and spin remain essentially unchanged until Mn is about one-third of the way between the cage center and edge, then decline significantly when Mn is shifted closer to the edge. We find that there are three energy minima on this path located from about 1 to 1.6 Å from the cage center, and, after the last energy minimum, the interaction between Mn and the cage turns repulsive (see Fig. 3). The spin is different at each local energy minimum, and decreases from $M=5.7$ to 5 then to 3, which corresponds to a change in electronic configurations of Mn from $(M=5.7)$ $[\text{Ar}]3d^{5.44}4s^{1.05}4p^{0.27}$ based on a DMOL3 calculation or $[\text{Ar}]3d^{5.13}4s^{0.52}4p^{0.22}$ based on a VASP calculation, to that of $(M=5)$ $[\text{Ar}]3d^{5.92}4s^{0.22}4p^{0.36}$ based on a DMOL3 calculation or $[\text{Ar}]3d^{5.82}4s^{0.30}4p^{0.53}$ based on a VASP calculation, respectively. Briefly stated, there are 0.24 or 0.50 Mn electrons moved to the cage based on VASP calculations. We also study the other two paths, and the behaviors are similar near the central region. However, there is only one energy minimum on each path, as shown in Fig. 3, and the spin is about 5 with similar electronic configuration as that of $M=5$ on path 3. We examine the energies on these three radial paths as well, and observe that path 3 has seemingly the lowest energy. Nevertheless we cannot be sure because of the insufficient resolution. As during the total energy calculations, Mn and C_{60} as a whole system are fixed, and the cage is optimized separately. Hence it is clear that this scheme is a good approximation only when Mn is located near the cage center; the whole system might be distorted slightly when Mn is close to the edge.

We then adopt a full optimization scheme using VASP at the PBE/PAW level. We start with various positions of Mn and allow the whole system to relax in total energy and spin. Although by controlling the step size of variation in Mn position, we are able to maintain Mn in the same path before and after optimization, we still examine the final Mn position after each optimization to be sure that Mn is indeed located on the path. As shown in Fig. 2, even though we start from different Mn positions, the system converges to several final states and each one has the same energy and spin. For example along path 3 we notice that there are three straight lines [the (red) diamond square at the origin is an isolated point], which correspond to $M=5.7$, 5, and 3, with a relative energy difference of 0.25 and 0.20 eV, where $M=3$ is the lowest in energy. Since they match well with those obtained using scheme 1, we attribute them to the local energy minima. For other two paths, we observe the similar features, except there is only one flat region, which corresponds to one

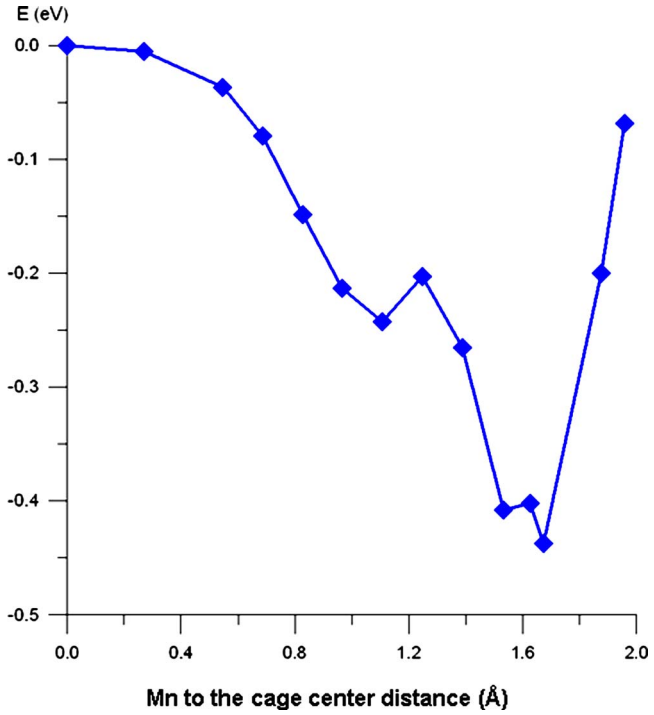

FIG. 4. (Color online) Total energy (eV) changes with Mn to the cage center distance (Å) along path 3 using scheme 3 (partial optimization). The total energy is set as zero when Mn is located at the cage center.

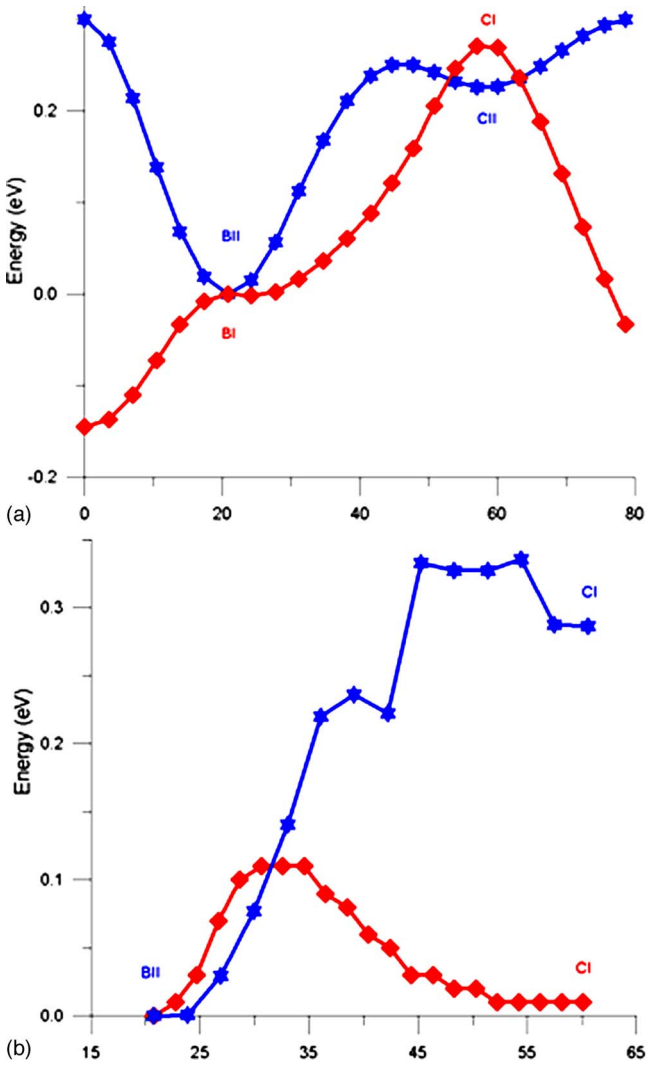

FIG. 5. (Color online) (a) Angular variation of total energy along the arc paths (see Fig. 1) from B_I to C_I (♦) with a radius of 1.2 Å and from B_{II} to C_{II} (⋆) with a radius of 1.625 Å using scheme 1. The energy range for the first arc path (♦) is multiplied by 30 to match that of the second arc path (⋆). Zero energy is chosen when Mn is located at positions B_I and B_{II} for each path, respectively. (b) Angular variation of total energy along the straight line path (see Fig. 1) from B_{II} to C_I using scheme 1 (♦) and using scheme 3 (⋆, partial optimization). Zero energy is chosen when Mn is located at position B_{II} for each scheme.

energy minimum on each path obtained using scheme 1. The most important finding at this point is that we are certain that path 3 is the one with the lowest energy, about 0.17 and 0.20 eV lower than those on paths 1 and 2, respectively. After full optimizations, we also compare the structures between when Mn is located at the cage center and global energy minimum, and we notice that the largest distortion in bond length (about 0.04 Å) occurs at a C═C double bond on the C_6 ring. Hence, in spite of the fact that the structure change is only a few percent, it is crucial to the ground state energy calculation. At the same time, we also use DMOL3 at the PBE/DNP level to verify the above results, and we find the similar qualitative feature on spin and energy orders except the energy differences between paths 1 and 2 are much smaller, 0.08 and 0.05 eV for paths 1 and 2, respectively.

To further study the energy change along path 3 and verify the fixed and full optimization schemes, we adopt a partial optimization scheme using the selective dynamics technique available in VASP at the PBE/PAW level, in which we only optimize one-half of the C_{60} while the other half of the cage and Mn are fixed. The energies are displayed in Fig. 4. The results resemble most of the features of those manifested in the previous section, namely, near the cage center, the energy surface is flat and $M=5.7$. There appears a shallow energy minimum where spin changes from $M=5.7$ to $M=5$ before the ground state. The ground state has Mn close to carbon atoms and spin $M=3$. This is further confirmation that Mn@C_{60} experiences different energy and spin states when Mn is shifted from the cage center to edge.

After having performed these calculations along paths 1–3, we adopt scheme 1 (we kept the carbon cage fixed during the total energy calculation) to investigate the angular variation of the total energy by introducing circular paths with radii from the cage center to local energy minima on the previous paths, shown in Figs. 1 and 3. For the three arc and straight line paths, we first show the arc path connecting the only energy minimum on path 2 and second energy minimum on path 3 in Fig. 5(a), that is, where radius $r=1.2$ Å (♦ curve). This path is located near the central region that has a flat energy surface, and the energy range of this path is only 0.01 eV. Recall as shown in Fig. 3 that both B_I and C_I are found to be local energy minima, and C_I is slightly higher in energy than B_I, ~0.01 eV. In the same figure, we present a path passing through the energy minimum on path 3, that is, where $r=1.6$ Å (⋆ curve). The energy range of this path is about 0.3 eV, approximately 30 times greater than that of the first arc path. We observe that B_{II} is a true energy minimum and is about 0.2 eV lower in energy than C_{II}. In order to plot the energies for the two arc paths together and assist in ease

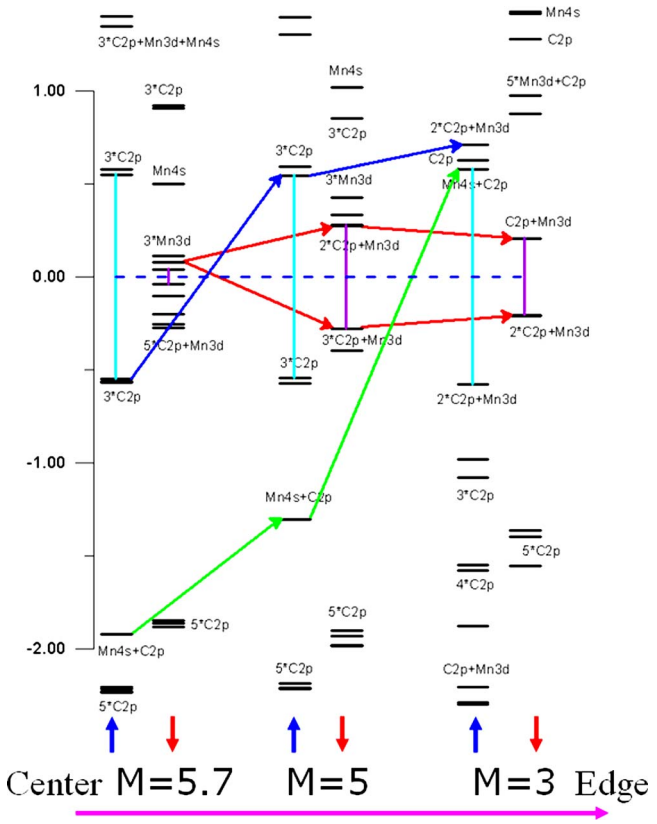

FIG. 6. (Color online) Molecular orbital energy diagrams for α and β spin electrons with different spins obtained using scheme 1. Zero energy is chosen to be the center of each HOMO-LUMO gap.

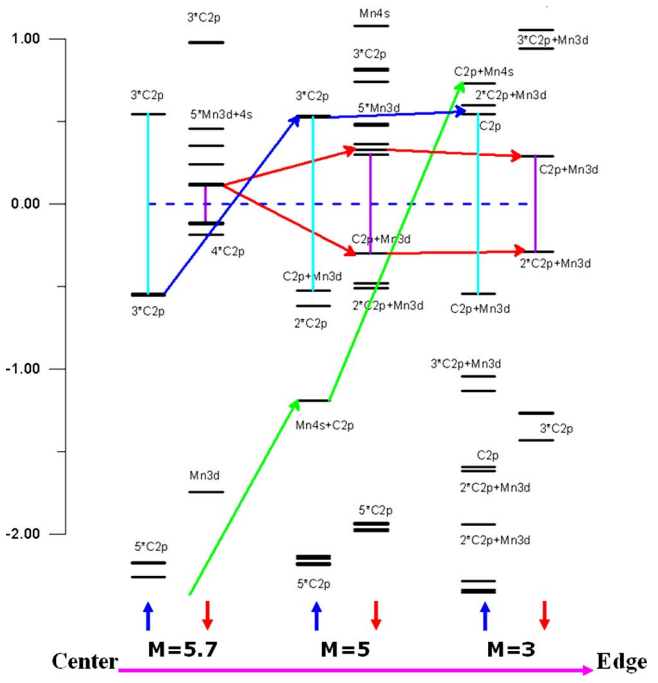

FIG. 7. (Color online) Molecular orbital energy diagrams for α and β spin electrons with different spins obtained using scheme 2. Zero energy is chosen to be the center of each HOMO-LUMO gap.

of viewing, we multiply the energy range of the first arc path by a factor of 30 and join the points B_{II} and C_I by a straight line. The results are presented in Fig. 5(b). We initially continue to use scheme 1, and notice that the (B_{II} and C_I) energies are close and there appears an energy barrier of 0.1 eV between them (♦ curve). Finally we utilize scheme 3 (partial optimization), that is, we fix one-half of the cage and Mn, then let the other half of the cage relax. The total energy is shown in the curve with ⋆. We notice that the energy difference is enlarged to about 0.29 eV, which is greater than that obtained previously, ~0.20 eV, using the full optimization scheme shown in Fig. 2. Furthermore, we observe that the spin M changes continuously from 3 to 5 when Mn is moved from B_{II} to C_I.

Having studied the total energy of Mn inside the carbon cage, we proceed to examine the electronic and spin configurations of the ground state (the energy minimum on each path). Here we present the orbital energy level diagrams of different spins from $M=5.7$ to 5 to 3, which correspond to moving Mn from the cage center to edge, obtained using schemes 1 and 2. As shown in Figs. 6 and 7 [(green) lines with arrow from Mn4s+C2p (spin ↑ and $M=5.7$) to Mn4s+C2p (spin ↑ and $M=5$) to Mn4s+C2p (spin ↑ and $M=3$) indicate the Mn4s orbital energy change; (blue) lines with arrow from 3*C2p (spin ↑ and $M=5.7$) to 3*C2p (spin ↑ and $M=5$) to 2*C2p+Mn3d (spin ↑ and $M=3$) indicate the C2p orbital energy change; (red) lines with arrow from 3*Mn3d (spin ↓ and $M=5.7$) to 3*C2p+Mn3d/2*C2p+Mn3d (spin ↓ and $M=5$) to 2*C2p+Mn3d/C2p+Mn3d (spin ↓ and $M=3$) indicate the Mn3d orbital energy change; vertical lines (purple) for spin ↓ at $M=5.7$, 5, and 3 indicate the β(HOMO-LUMO) (HOMO denotes highest occupied molecular orbital; LUMO denotes lowest unoccupied molecular orbital) gap; and vertical lines (light blue) for spin ↑ at $M=5.7$, 5, and 3 indicate the α(HOMO-LUMO) gap], we find that they are qualitatively similar. However, we notice several prominent changes. First, for the α (spin ↑) orbitals, the originally occupied three C2p orbitals (Mn at the cage center) rise in energy due to increasing interaction with the cage and become unoccupied states [following the line with arrow (blue arrows) for C2p orbital energy change]. Similarly, the hybridized state Mn4s+C2p also increases in energy and becomes an unoccupied state [following the line with arrow (green arrows) for Mn4s+C2p orbital energy change] as well. For the β (spin ↓) orbitals the originally unoccupied five Mn3d states (Mn at the cage center) mix with C2p states of the cage. Some of the resultant orbitals rise in energy and remain unoccupied but others decrease in energy and become occupied [following the lines with arrow (red arrows) for Mn3d orbital energy change]. The α(HOMO-LUMO) gaps remain almost constant, ~1.1 eV, in the course of moving Mn from the cage center to ground state [α(HOMO-LUMO) gap (light blue) vertical lines], but the β(HOMO-LUMO) gaps increase from 0.2 to 0.6 eV [β(HOMO-LUMO) gap (purple) vertical lines], which prevents the α and the β electrons from being excited to orbitals at higher energy levels, and this increase in the HOMO-LUMO energy gap fosters Mn@C_{60} evolving into a stable state as Mn is moved off the cage center. In Fig. 8, we show the deformation electron density (total electron density minus electron density of atoms) when Mn is located at its ground state. The excess

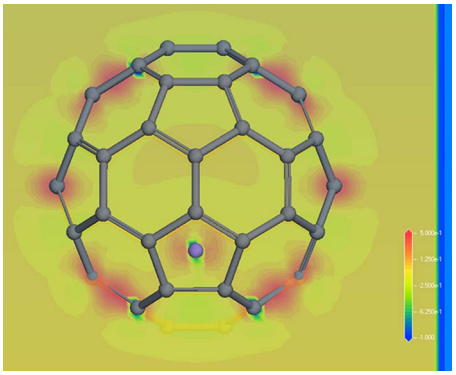

FIG. 8. (Color online) Deformation electron density contour plot for the ground state of $Mn@C_{60}$.

charge is primarily residing on Mn and a few nearby carbon atoms. This charge distribution indicates that the interaction between Mn and C_{60} is electrostatic in nature. Detailed analysis on occupations of molecular orbitals reveals that some of the orbitals nearby the HOMO are partially occupied. Furthermore, using the G03 we deduce the total dipole moment at the ground state to be 5.14 D. Since the total spin is 3, the spin populations on Mn and C_{60} are 1.8 and 1.2, respectively. Also based on Mulliken population analysis obtained using VASP for the ground state, we find that the occupied molecular orbitals of the ground state are composed of Mn3*d* and C2*p* atomic orbitals caused by hybridization, which raises the energy of C2*p* and Mn4*s* levels, but lowers that of Mn3*d*. Specifically, we notice that the HOMO and LUMO (both α and β) are derived from one of the C_{60} orbitals (C2*p*) and contained components from Mn3*d*. The HOMO α and β are $0.473C2p+0.327Mn3d$ and $0.495C2p+0.269Mn3d$, respectively, while the LUMO α and β are $0.570C2p+0.060Mn3d$ and $0.504C2p+0.237Mn3d$, respectively. Hence it is clear that the α(LUMO) is mainly C2*p*, and β(LUMO) is strongly hybridized.

IV. CONCLUSION

In summary, we study the behavior of a Manganese atom encapsulated inside a C_{60} using density functional theory with the generalized gradient approximation. We carry out the calculations through three optimization schemes and along four paths inside the cage. We note that when Mn is located near the cage center, it is weakly bound to the cage due to electrostatic interactions. When Mn is shifted from the cage center to edge, the total energy and spin start to decrease significantly around one-third of the radius of the fullerene and subsequently the total energy reaches a local minimum. When Mn is further moved toward the edge, the interaction becomes repulsive. With the support of results from our systematic calculations, we conclude that the global energy minimum is located about 1.6 Å away from the cage center and right above the C_6 ring with spin $M=3$. The binding energy of $Mn@C_{60}$ is 0.08 eV, and the energy order (eV) for different Mn positions inside C_{60} is as follows: $Mn@C_{60}$ (ground state, a path 3 local minimum, −0.08, stable) $<C_{60}$ +Mn (separate, 0) $<Mn@C_{60}$ (path 1 local minimum, 0.09, unstable) $<Mn@C_{60}$ (path 2 local minimum, 0.13, unstable) $<Mn@C_{60}$ (I_h, cage center, 0.33, unstable). Moreover, based on Mulliken population analysis, we deduce the orbital composition of the ground state and attribute the decrease in total energy and spin to Mn and C hybridization which increases the orbital energies of C-2*p* and Mn-4*s* while decreases those of Mn-3*d*.

ACKNOWLEDGMENTS

This work was supported by Nebraska Research Initiative (No. 4132050400). JL thanks the grants from the NSFC (Grant Nos. 1074003, 10474123, 10434010, 90606023, 20731160012), and National 973 Project (Nos. 2002CB613505 and 2007CB936200, MOST of China). We appreciate Professor Ian Hamilton for proofreading the paper and helpful comments.

[1] J. R. Heath, S. C. O'Brien, Q. Zhang, Y. Liu, R. F. Curl, H. W. Kroto, F. K. Tittel, and R. E. Smalley, J. Am. Chem. Soc. **107**, 7779 (1985).
[2] R. Tellgmann, N. Krawez, S.-H. Li, I. V. Hertel, and E. E. B. Campbell, Nature (London) **382**, 407 (1996).
[3] S. Nagao, T. Kurikawa, K. Miyajima, A. Nakajima, and K. Kaya, J. Phys. Chem. A **102**, 4495 (1998).
[4] J. Lu, W. N. Mei, Yi Gao, X. Zeng, M. Jing, G. Li, R. Sabirianov, Z. Gao, L. You, J. Xu, D. Yu, and H. Ye, Chem. Phys. Lett. **425**, 82 (2006).
[5] J. Lu, R. F. Sabirianov, W. N. Mei, Yi Gao, C.-G. Duan, and X. Zeng, J. Phys. Chem. B **110**, 23637 (2006).
[6] A. H. H. Chang, W. C. Emler, and R. M. Pitzer, J. Chem. Phys. **94**, 5004 (1991).
[7] J. Lu, L. Ge, X. W. Zhang, and X. Zhao, Mod. Phys. Lett. B **13**, 97 (1999).
[8] K. Laasonen, W. Andreoni, and M. Parrinello, Science **258**, 1916 (1992).
[9] W. Andreoni and A. Curioni, *Int. Winter School on Electron. Properties of Novel Materials: Prog. Fullerene Research*, 2nd ed. (World Scientific, River Edge, NJ, 1994), p. 93.
[10] W. Andreoni and A. Curioni, Appl. Phys. A: Mater. Sci. Process. **66**, 299 (1998).
[11] V. N. Ivanova, J. Struct. Chem. **41**, 135 (2000).
[12] K. Ranjan, K. Dharamvir, and V. K. Jindal, Indian J. Pure Appl. Phys. **43**, 654 (2005).
[13] GAUSSIAN 03, Revision D.01, M. J. Frisch, G. W. Trucks, H. B. Schlegel *et al.*, Gaussian, Inc., Wallingford CT, 2004.
[14] A. D. Becke, J. J. Chem. Phys. **98**, 5648 (1993).
[15] C. Lee, W. Yang, and R. G. Parr, Phys. Rev. B **37**, 785 (1988).
[16] G. Kresse and J. Hafner, Phys. Rev. B **47**, 558 (1993).
[17] G. Kresse and J. Hafner, Phys. Rev. B **49**, 14251 (1994).
[18] G. Kresse and J. Furthmüller, Comput. Mater. Sci. **6**, 15 (1996).
[19] G. Kresse and J. Furthmüller, Phys. Rev. B **54**, 11169 (1996).
[20] G. Kresse and J. Hafner, J. Phys.: Condens. Matter **6**, 8245 (1994).
[21] B. Delley, J. Chem. Phys. **92**, 508 (1990).
[22] B. Delley, J. Chem. Phys. **113**, 7756 (2000).
[23] J. P. Perdew, K. Burke, and M. Ernzerhof, Phys. Rev. Lett. **77**, 3865 (1996).
[24] J. P. Perdew, K. Burke, and M. Ernzerhof, Phys. Rev. Lett. **78**, 1396 (1997).
[25] P. E. Blöchl, Phys. Rev. B **50**, 17953 (1994).
[26] G. Kresse and J. Joubert, Phys. Rev. B **59**, 1758 (1999).
[27] DNP=double-numeric quality basis set with polarization functions, i.e., functions with angular momentum one higher than that of highest occupied orbital in free atom. DNP is available in DMOL3.